Modeling and implementing power electronics systems for solar powered RC planes

Marvin Exalto, Athul Perumpillichira

4370090, 4448588

Bachelor thesis

TU Delft Delft University of Technology

Modeling and implementing power electronics systems for solar powered RC planes

Bachelor thesis

Marvin Exalto, Athul Perumpillichira

4370090, 4448588

July 19, 2019

Faculty of Electrical Engineering, Mathematics and Computer Science (EEMCS)
Delft University of Technology


TU Delft
Delft
University of
Technology

Abstract

This BSc thesis concerns the solar plane bachelor graduation project. This project aims to improve the flight time of a commercially available RC plane by utilizing photovoltaic technologies. In this thesis the power electronics system that supplies power generated by photovoltaic technologies to the RC plane used during the solar plane project will be designed, modeled, implemented and tested.

Utilizing Matlab Simulink, the power usage and generation of the solar plane is modeled and simulated. The final simulink model is used to determine the performance of the plane by ways of predefined performance parameters. This model shows that for the chosen RC plane of the solar plane project, flight times equal to 16.76 times its initial flight time can be achieved if the plane is flown during the day. Under a constant irradiance of 800 W/m^2, even continuous flight is possible.

The implementation of this power electronics system is tested both as a stand alone system and on the solar plane during flight. The system shows an efficiency of 85% to 90% for power conversion at an input power of 10+ Watts.

Preface

This thesis concerns the BSc graduation project conducted at the Delft University of Technology, under the supervision of Dr. Olindo Isabella. The project group consisted of six members and was divided in three subgroups of two members, each with their own tasks and responsibilities. The goal of the project was the development of a system capable of powering a RC plane utilizing photovoltaic technologies.

In this thesis, the design and implementation choices made by the power electronics subgroup of the solar plane project are presented and the obtained results are discussed. It is our sincere hope that the information presented in this thesis will inform and inspire anyone who may read this thesis.

Contents

Introduction

Unmanned aerial vehicles (UAVs) are a booming technology with a myriad of potential applications. Solar panels can be installed on UAVs in order to extend the flying time and/or range. These solar planes are already being used to monitor and map a big crevasse in the arctic Bowdoin Glacier [8], to gather data to build better models to predict the effects of climate change. While there is great interest in solar plane technology, there are technical challenges to be tackled. The main design objective of the power system is to achieve very high energy efficiency and keep the design lightweight.

The solar plane project aims to develop a system for a commercially available RC plane that is capable of extending its flight time by utilizing photovoltaic (PV) modules. For the development of this system the power electronics subgroup will model and develop the necessary systems needed to provide power to the plane by utilizing PV modules.

In this chapter the problem definition, key concepts of flight dynamics and PV systems for solar planes will be introduced. These concepts will serve as the basis of the design and model of the power electronics (PE) system. Finally, the structure of the thesis will be presented.

1-1 Problem definition

During the solar plane project, the project group will design the electric system of the solar plane and choose appropriate PV technology. The first step is selecting very lightweight high-efficiency solar panels, and calculating how much power can be gained from the available area. Based on the connection of the PV modules appropriate power electronic converter will be chosen to implement maximum power point tracking (MPPT) and interface the PV modules with the battery and the motor. Moreover, the MPPT must be able to track changes quickly without losing the optimal point.

The power electronics subgroup of the solar plane project is in charge of the design, modeling, implementation and testing of the power electronics system. This includes the modeling and circuit implementation of the MPPT, converters and battery unit.

1-2 PV systems for solar planes

In this subsection concepts regarding the design of PV systems in the context of solar planes will be presented and analyzed. These concepts will be used throughout the thesis to successfully design and implement a power electronics system for the solar plane project.

PV systems can vary from small and simplistic to big and complex depending on the amount of power that it needs to be supply to its load for both grid and non-grid connected loads.[4] Figure 1-1 illustrates an example of an off-grid PV system with battery storage units and both AC and DC loads. Figure 1-2 shows a PV system schematic representation for a solar plane.

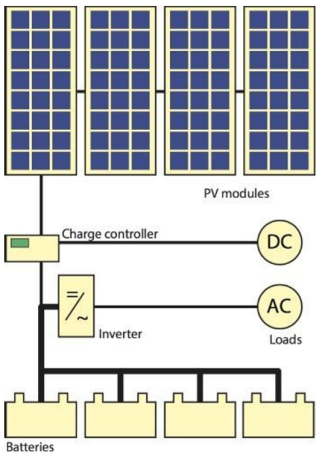

Figure 1-1: Schematic representation of a complex PV system including batteries, power conditioners, and both DC and AC loads. [4]

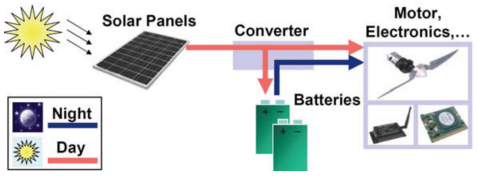

Figure 1-2: Schematic representation of PV system used for a solar plane.[1]

In the event that the PV modules generate more power then is required by the load at that moment, the excess power generated can be used to store energy in a storage unit. In order for this to work correctly, a charge controller is needed. In [5] a design for a charge controller is given.

Many PV systems are equipped with a so called maximum power point tracker (MPPT), with this module the output power of the PV modules can be maximized. A MPPT is never an actual component itself but always connected to a DC-DC converter in a PV inverter or a charge controller. [4] MPPTs can be implemented using various algorithms, each with their own advantages and disadvantages [9] [2] [3].

1-3 Structure of thesis

The structure of this thesis is as follows. Chapter 2 will define the specifications for both the entire plane and the power electronics system. Chapter 3 will present the design of the power electronics system used to meet the systems specifications. Chapter 4 will present the model used to simulate the design of the plane as well as define various performance parameters. Chapter 5 will present the circuit level implementation of the power electronics system design. Chapter 6 will present the obtained simulation and test results of the final system. Finally, Chapter 7 will give the conclusion of the thesis followed by possible improvements and future work regarding the power electronics system of the solar plane.

Program of requirements

The solar plane project group is divided into three separate subgroups each with their own. The three subgroups are: PV, power electronics and control subgroup. Each of the systems developed by the subgroups will be combined in order to realize the common goal of the project, the creation of a solar plane.

In this chapter the program of requirements for the entire solar plane system and power electronics system will be presented. These specifications will be used for the design and implementation of the power electronics system.

2-1 Specifications of entire RC plane

The specifications of the system developed for the solar plane project are based on the research objectives stated in the initial proposal for the project:

P1. The plane, with all its onboard components, must be able to fly.

P2. The generation of power by utilizing onboard PV modules.

P3. The system must increase the flight time of the RC plane

2-2 Specifications for the power electronics system

The power electronics subgroup must ensure that the whole system is electrically compatible and maximize the efficiency of the electrical power transfer. As a result, the power electronics subgroup of the solar plane project is in charge of:

- Modeling of the power generation and usage of the plane components during flight.
- Design and implementation of the power electronics system.

The model of the solar plane components will be used to predict the performance of the solar plane configuration. This model is developed such that the following specifications are uphold.

M1. Determine the possibility of flight of the solar plane.

M2. Determine the power generation and usage of all onboard components.

M3. Determine the total flight time of the solar plane and flight time improvement compared to an equivalent plane without solar power system.

The implementation of the power electronics system will operate directly with both the PV and control subsystems and is therefore dependent on the input and output characteristics of these subsystems. The implementation of the power electronics system must conform to the following specifications.

I1. Supply power generated by the PV modules on the plane to the plane components.

1. The input of the system must accept an input voltage range of $5V$ to $7.4V$ and current range of $0A$ to $4A$ from the PV modules.
2. The output of the system needs to supply the plane load with a voltage ranging from of $6.8V$ to $7.5V$.

I2. Maximize the power output of the PV modules.

1. The implementation of the module that maximizes the PV module power must operate at an efficiency of at least 85% for the given voltage and current ranges of specification I1.
2. The implementation of the module must be a lightweight as possible.

I3. Maximize the energy efficiency of the entire system.

1. Energy generated by the PV modules that is not used to power the plane must be stored.

Power electronics system design

Given in figure 3-1 is an overview of the main component groups of the solar plane project, the power electronics subgroup will mainly focus on the MPPT, charge controller and battery. These component groups are designed and implemented during the solar plane project such that the specifications in section 2-1 are met successfully.

In this chapter the high level design of the power electronics system used to meet the specifications given in section 2-2 will be presented. The designed system will be based on an off-grid PV system as illustrated and introduced in figure 1-1 and section 1-2 and [10]. This system will be able to provide power from the PV modules to the plane load while maximizing PV power output and energy efficiency of the system.

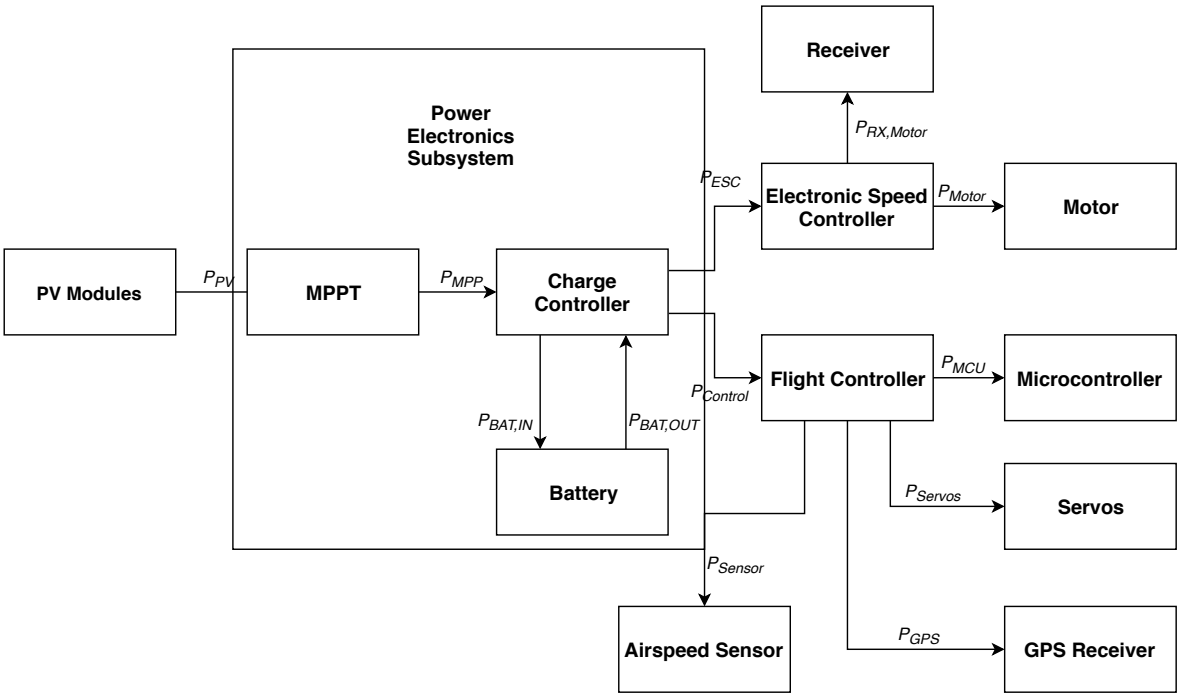

Figure 3-1: High level design schematic of the power electronics system as part of the complete solar plane system.

3-1 Maximizing PV power output utilizing maximum power point tracker

In this section the design of the MPPT module will be presented.

The MPPT module will receive a voltage and current at its input within the range specified in specification I1.1 and must convert this to the output range specified in specification I1.2. For the MPPT module to successfully meet the specifications it must be equipped with a voltage and current sensor as well as a DC/DC converter. The conceptual design of the MPPT module is given in figure 3-2.

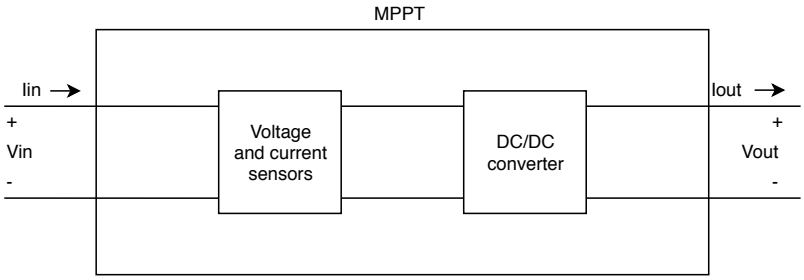

Figure 3-2: Conceptual design of MPPT module

3-2 Maintaining correct battery voltage by utilizing a charge controller

In this section the charge controller and battery modules used to maximize energy efficiency of the power electronics system in order to conform to specification 3 given in section 2-2 is designed.

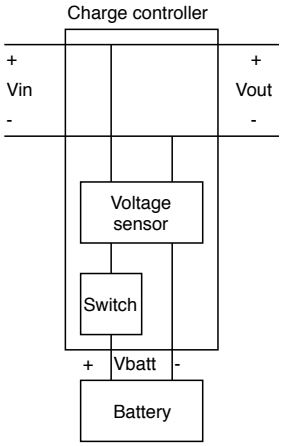

Figure 3-3: Conceptual design of charge controller module

The charge controller is designed to disconnect the battery from the PV power output when the state of charge has reached its safe limit. As designing and constructing a battery are outside the scope of this project, an off-the-shelf battery pack will be purchased and used.

3-3 Conclusion and discussion of power electronics system design

The aim of the solar plane project is to increase the flight time of a RC plane by utilizing PV modules. To achieve this a power electronics system is needed that can supply the power demand of the plane utilizing both the power of the PV modules as well as the power available from the onboard battery.

The high level design schematic of the system used to achieve this is given in figure 3-1. In this system a maximum power point tracker (MPPT) is used to maximize the power output of the PV modules and a charge controller is used to charge or discharge the battery in order to provide the power load of the plane depending on power demand and generation. The conceptual design of the power electronics system is given in figure 3-4

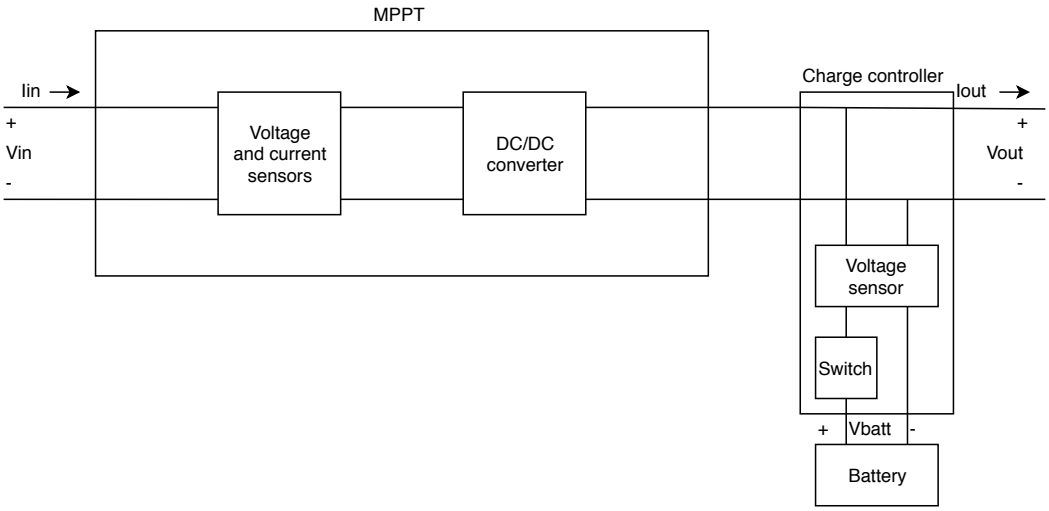

Figure 3-4: Conceptual design of power electronics system

Power electronics system modeling for solar powered RC planes

In this chapter the designed power electronics system of chapter 3, given in figure 3-1, used to supply the load of the plane using power generated with PV modules will be modeled following specification M1 to M3 given in section 2-2. This will be done by calculating the power usage of the plane load and power supply of the MPPT and battery. All modeled Simulink subsystems of the power electronics system will be combined in order to model the complete power electronics system. Using the obtained models of the plane power usage, the minimum and maximum flight speed will be calculated and performance parameters used to determine the flight performance and energy efficiency of the plane will be defined. Finally, based on the obtained model, design considerations for the design of the plane will be presented.

4-1 Power electronics modeling during level flight

In this section the model used to simulate the power electronics system, as presented in figure 3-1, will be modeled using Simulink. First the power usage and generation each subsystem will be modeled individually, each subsystem will then be combined in order to create the complete power electronics system model.

4-1-1 Modeling power usage of plane load during level flight

During the entire operation duration of the solar plane, the power supplied by the PV modules and battery must equal the power demand of the plane load. In order to model the performance of the power electronics system the power demand and losses of the plane load must be known. In this subsection, the power demand of the plane load during level flight will be calculated and a model of the plane load will be implemented using Simulink.

Let m be the total mass of the solar plane equipped with all necessary equipment, A_{wings} be the total surface area of the plane wings, C_D and C_L be the drag and lift coefficients of the plane respectively, g be the gravity acceleration and ρ be the density of air at the flight altitude. The propulsion power needed to maintain level flight P_{level} is then calculated using equation 4-1. [1]

$$P_{level} = \frac{C_D}{C_L^{3/2}} \sqrt{\frac{2(mg)^3}{\rho A_{wings}}} \tag{4-1}$$

The total mass of the plane m is the sum of the airplane frame mass m_{frame}, the combined total weight of electrical equipment and circuitry m_{elec}, the weight of the battery m_{batt} and the weight and area of the installed PV modules m_{PV}. Mass m is then calculated using equation 4-2.

$$m = m_{frame} + m_{elec} + m_{batt} + m_{PV} \tag{4-2}$$

The mass of the PV modules m_{PV} is determined by the total area of the plane wings covered and the density of PV modules. Let A_{PV} and ρ_{PV} be the area and density of the PV modules respectively. Then m_{PV} is calculated by equation.

$$m_{PV} = \rho_{PV} A_{PV} \tag{4-3}$$

The power delivered to the plane is subject to power inefficiencies of the various pieces of propulsion hardware on the plane, let n_{plane} be the combined power use efficiency of all onboard motor equipment of the plane. Let $P_{electronics}$ be the power usage of the onboard electronics, then the total power that needs to be provided by the battery and PV system to the plane load P_{load} is then calculated using equation 4-4. Equation 4-4 is implemented using Simulink according to figure 4-1.

$$P_{plane} = \frac{P_{level}}{n_{plane}} + P_{electronics} \tag{4-4}$$

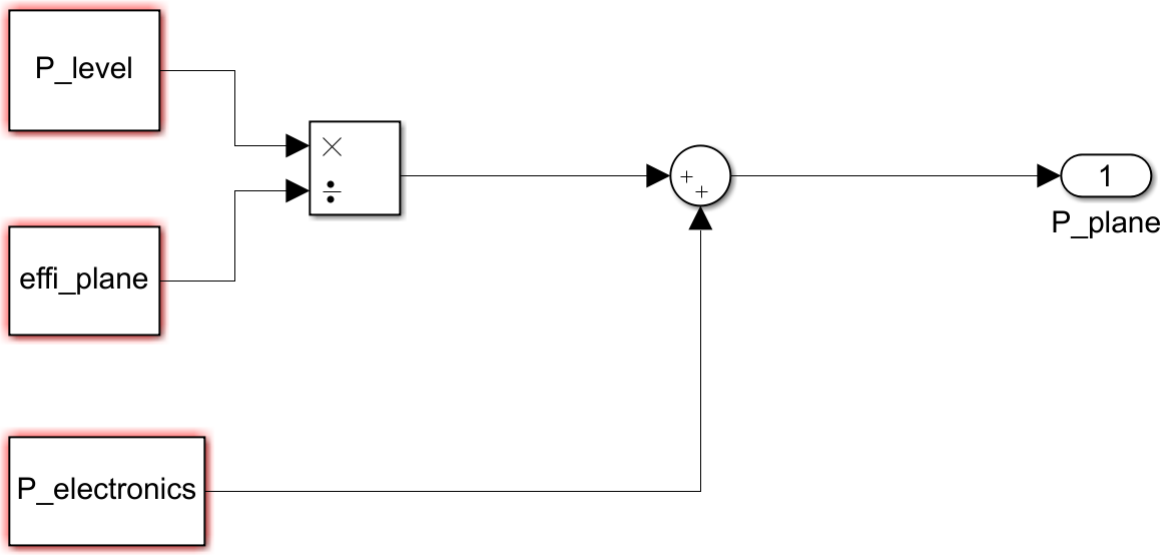

Figure 4-1: Simulink implementation of plane load model.

4-1-2 PV module power generation modeling and MPPT

Onboard PV modules will supply the solar plane with power. In order to maximize the power output of the PV modules a MPPT is used. In this subsection the model used to simulate the

power generated generated by the PV modules and MPPT will be designed and implemented using Matlab Simulink.

Let $k_{PVcover}$ be the percentage of wing area covered with PV modules. The total area of PV modules on the wings A_{PV} is then calculated using equation 4-5. Let $I(t)$ be the irradiance of light upon the the PV modules as a function of time t and n_{PV} be the power efficiency of the of the PV modules. The maximum power generated by the PV modules on the wings as a function of time $P_{PV}(t)$ is then calculated using equation 4-6. The Simulink model of the PV module subsystem is given in figure 4-2.

$$A_{PV} = k_{PVcover} A_{wings} \tag{4-5}$$

$$P_{PV}(t) = n_{PV} A_{PV} I(t) \tag{4-6}$$

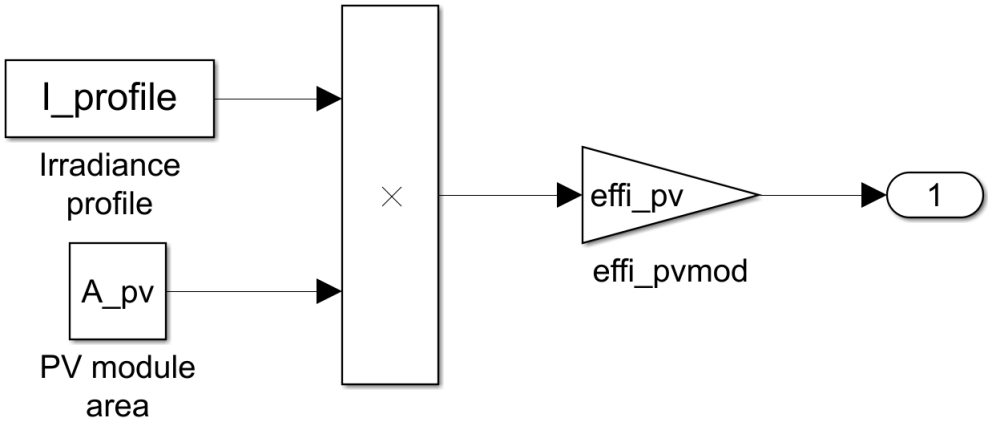

Figure 4-2: Simulink implementation of PV module model.

The MPPT is subject to power usage inefficiencies, the simulink model of the MPPT can be implemented utilizing only a gain block. Let n_{mppt} be the power efficiency of the MPPT. The simulink implementation of the MPPT is then given by a gain block with value n_{mppt}

4-1-3 Battery modeling and charge controller

The onboard charge controller will charge and discharge the battery depending on power supply and demand. In this subsection a model of the plane battery will be presented and the charge controller algorithm used for the simulation will be implemented using Simulink.

The battery used in the RC plane is implemented in Simulink using the standard Simulink battery model, the implementation of the battery in Simulink is given in figure 4-3. The charge and discharge efficiencies of the battery are defined as n_{charge} and $n_{discharge}$.

Determining when the battery is charged and discharged is done by the charge controller. The charge controller measures the generated power of the PV modules and battery, state of charge of the battery and demanded power of the plane load. This controller is implemented in Simulink using algorithm A-3-1.

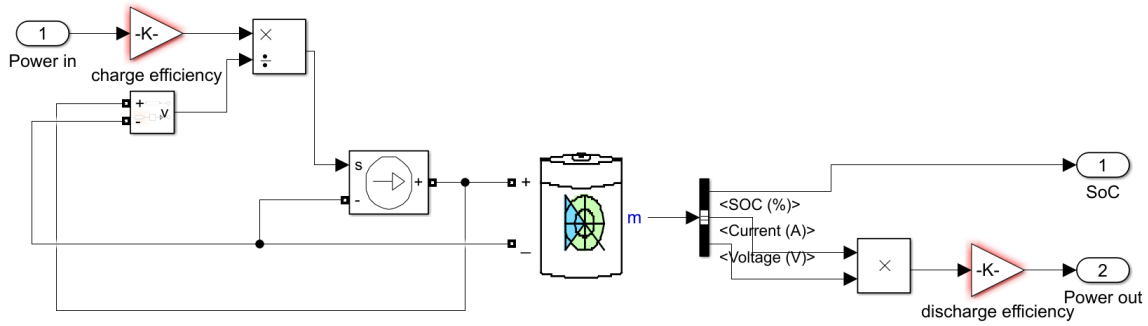

Figure 4-3: Simulink implementation of battery.

4-1-4 Complete power electronics system modeling

All subsystems are combined according to the design given in figure 3-1 to form the power electronics simulink model given in figure 4-4. With this model it is possible to simulate the performance of the power electronics system for various irradiance profiles. The model returns the power supply of the PV modules and batttery and the state of charge of the battery as a function of time.

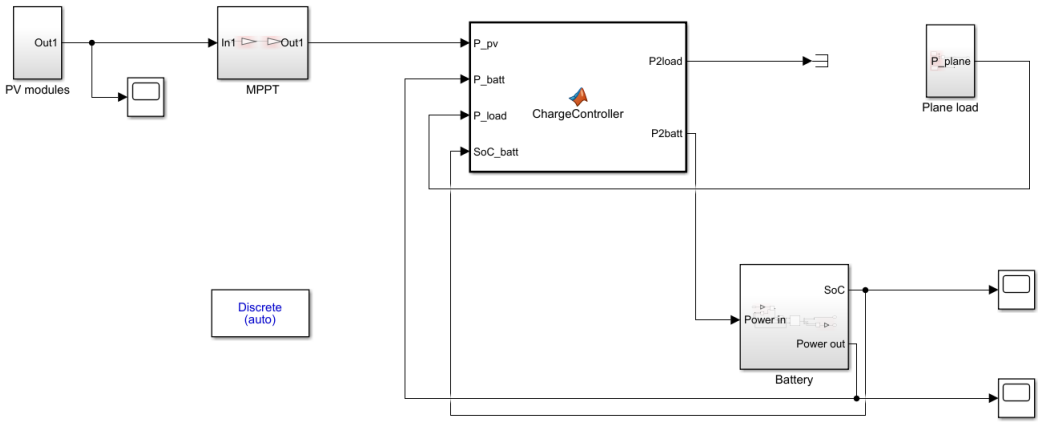

Figure 4-4: Simulink implementation of complete power electronics system.

4-2 Flight speed modeling

In this section the minimum speed required to achieve level flight and the maximum speed achievable of the plane will be calculated.

4-2-1 Calculating minimum velocity at level flight

In this subsection the minimum velocity required to maintain level flight is calculated.

The powers P_{lift} and P_{drag} due to the lift and drag forces on the plane are given in equations 4-7 and 4-8 respectively.

$$P_{lift} = \frac{1}{2}\frac{(mg)^2}{A_{lift}\rho v} \tag{4-7}$$

$$P_{drag} = \frac{1}{2}C_D\rho A_{front}v^3 \tag{4-8}$$

Let F_{lift} be the lift force on the plane during level flight and A_{lift} be the surface upon which the lift force acts, then the lift coefficient C_L is given by equation 4-9.

$$C_L = \frac{2F_{lift}}{A_{lift}\rho v^2} = \frac{2mg}{A_{lift}\rho v^2} \tag{4-9}$$

The power during level flight at velocity v is then given by equation 4-10.

$$P(v) = P_{lift} + P_{drag} = \frac{1}{2}\frac{(mg)^2}{A_{lift}\rho v} + \frac{1}{2}C_D\rho A_{front}v^3 = \frac{1}{2}\left(\frac{1}{2}C_L mgv + C_d\rho A_{front}v^3\right) \tag{4-10}$$

Let v_{min} be the minimum velocity needed for level flight. By equating equations 4-1 and 4-10 at v_{min} yields equation 4-11. Solving this equality for v_{min} will give the minimum velocity needed for level flight.

$$P(v_{min}) = P_{level} \tag{4-11}$$

4-2-2 Calculating maximum possible flight velocity

In this subsection the maximum possible velocity of the solar plane is calculated.

Let $F_{thrust,max}$ be the maximum thrust force that can be provided by the plane propulsion system and v_{max} be the flight velocity of the plane when the propulsion system is providing its maximum thrust force. The power used by the propulsion system at maximum thrust $P_{thrust,max}$ is then calculated using equation 4-12.

$$P_{thrust,max} = F_{thrust,max}v_{max} \tag{4-12}$$

Equating equations 4-12 and 4-10 such that $P_{thrust,max} = P(v_{max})$ and solving for v_{max} calculates the maximum possible velocity given in equation 4-13.

$$v_{max} = \sqrt{\frac{F_{thrust,max} - \frac{1}{4}C_L mg}{\frac{1}{2}C_d\rho A_{front}}} \tag{4-13}$$

4-3 Solar plane performance parameters

Given in section 2-1 are the solar plane specifications that need to be met for the successful completion of the solar plane project. In order to determine if a given RC plane will meet these specifications, appropriate performance parameters are required. In this subsection the performance parameters used to determine the performance of the solar plane will be defined. These parameters will determine if a given solar plane is able to meet project specifications P1 and P3 given in section 2-1.

4-3-1 Possibility of flight

In this subsection the parameter used to determine the possibility of flight in order to satisfy specification P1 of section 2-1.

The ability of the plane to fly depends on the thrust force output of the onboard motor, the ability of flight is guaranteed if and only if the motor is able to provide the necessary thrust needed to reach v_{min}. Based on equation 4-13, it can be determined that the possibility of flight can only be true when $v_{min} < v_{max}$. This inequality leads to equation 4-14 which will be defined as the possibility of flight parameter. If this equation holds true, specification P1 is considered to be satisfied

$$v_{min} < \sqrt{\frac{F_{thrust,max} - \frac{1}{4}C_L mg}{\frac{1}{2}C_d \rho A_{front}}} \tag{4-14}$$

4-3-2 Total flight time

In this subsection the parameter used to determine the flight time improvement of the solar plane, in order to determine if specification P3 of section 2-1 is met, is defined.

Let SOC_{max} and SOC_{min} be the maximum and minimum state of charge of the battery, C_{batt} be the energy capacity of the battery, V_{batt} be the nominal output voltage of the battery and $P_{plane,noPV}$ be the plane power requirement when $m_{PV} = 0kg$. The flight time of the solar plane when no PV power is generated during the duration of the flight $T_{flight,noPV}$ is then calculated using 4-15.

$$T_{flight,noPV} = \frac{(SOC_{max} - SOC_{min})C_{batt}V_{batt}}{P_{plane,noPV}} \tag{4-15}$$

Considering the solar plane during flight given a certain irradiance profile $I(t)$ and initial battery state of charge SOC_{start}. The power supplied by the battery is then calculated by equation 4-16. The energy stored in the battery during flight as a function of time $E_{batt}(t)$ is then calculated by equation 4-17.

$$P_{batt}(t) = \begin{cases} n_{discharge}(P_{load} - P_{PV}(t)) & \text{if } P_{load} > P_{PV}(t) \\ n_{charge}(P_{load} - P_{PV}(t)) & \text{if } P_{load} \leq P_{PV}(t) \end{cases} \tag{4-16}$$

$$E_{batt}(t) = SOC_{start} C_{batt} V_{batt} - \int_0^t P_{batt}(\tau) d\tau \tag{4-17}$$

The total flight time of the solar plane T_{flight} is defined as the time interval between the start of the flight until the state of charge of the battery reaches $SOC(t) = SOC_{min}$. The total flight time is then calculated by solving equation 4-18 for T_{flight}.

$$E_{batt}(T_{flight}) = SOC_{min} C_{batt} V_{batt} \tag{4-18}$$

The flight time improvement performance parameter $r_{T,improve}$ is then defined by equation 4-19. When equation 4-19 is greater then one, specification P3 of section 2-1 is satisfied

$$r_{T,improve} = \frac{T_{flight}}{T_{flight,noPV}} \tag{4-19}$$

4-4 Solar plane design considerations

Excluding the performance parameters defined by equations 4-14 and 4-19 used to satisfy specifications P1 and P3 of section 2-1, other design criteria can be defined for the performance of the solar plane. In this section various design considerations for plane component selection will be defined which can be used to optimize the design of the solar plane.

4-4-1 Battery considerations

As described by equation 4-2 the total mass of the plane depends partly on the mass of the battery while equation 4-1 shows that the power demand increases as the mass increases. It is therefore prefered to choose a battery with a high and energy and power density $E_{density}$ and $P_{density}$ as defined by equations 4-20 and 4-21 respectively.

$$E_{density} = \frac{C_{batt}}{m_{batt}} \tag{4-20}$$

$$P_{density} = \frac{P_{discharge,max}}{m_{batt}} \tag{4-21}$$

4-4-2 Wing aspect ratio

Given a plane with rectangular wings, let L_{wings} and W_{wings} be the length and width of the plane wings. The approximate aspect ratio of the plane wings R_{aspect} is then defined by equation 4-22. Substitution of equation 4-22 into equation 4-1 yields equation 4-23, this equation shows that for P_{level} to be minimized the plane must have a low R_{aspect} value and high L_{wings} value.

$$R_{aspect} = \frac{L_{wings}}{W_{wings}} = \frac{L_{wings}}{A_{wings}/L_{wings}} = \frac{L_{wings}^2}{A_{wings}} \tag{4-22}$$

$$P_{level} = \frac{C_D}{C_L^{3/2}} \sqrt{\frac{2R_{aspect}(mg)^3}{\rho L_{wings}^2}} \tag{4-23}$$

4-4-3 Wasted surplus power generation

In the event that $n_{mppt}P_{PV} > P_{plane}$ when the battery state of charge $SOC = SOC_{max}$, the part of the generated PV power that can not be used to supply the plane load or charge the battery is defined as $P_{waste}(t) = n_{mppt}P_{PV}(t) - P_{plane}$. This surplus power generated is considered to be wasted.

Let $T_1 \leq t \leq T_2$ be a time interval during which $n_{mppt}P_{PV} > P_{plane}$ and $SOC = SOC_{max}$ is true. The wasted energy over this time interval E_{waste} is then calculated by equation 4-24.

$$E_{waste} = \int_{T_1}^{T_2} P_{waste}(t)dt = \int_{T_1}^{T_2} n_{mppt}P_{PV}(t) - P_{plane}dt \tag{4-24}$$

Let N be the total amount of time intervals during which $n_{mppt}P_{PV} > P_{plane}$ over the entire duration of the flight. The performance parameter used to determine the ratio of wasted energy compared to the PV module energy generation over the entire entire flight time due to surplus power generation k_{waste} is then defined by equation 4-25. For the energy efficiency of the solar plane to be maximized, the solar plane is desired to be designed such that k_{waste} equals zero.

$$k_{waste} = \frac{\sum_{i=1}^{N} E_{waste,i}}{E_{PV}} = \frac{\sum_{i=1}^{N} E_{waste,i}}{\int_0^{T_{flight}} n_{mppt}P_{PV}(t)dt} \tag{4-25}$$

4-5 Conclusion and discussion of obtained system model

In this chapter the plane power usage model, performance parameters and design considerations were defined. The model and performance parameters will be used in chapter 6 to determine the performance of the final solar plane design.

In section 4-1 the power usage and generation of the solar plane were calculated in order to model the power electronics system according to model specifications M1 to M3 of section 2-2. Given in figure 4-4 is the complete power electronics system simulink model. This model can be used to determine:

1. Plane power usage during level flight
2. PV module power generation over time
3. Battery charge and discharge power

4. Battery state of charge measurement
5. Total flight time

Section 4-2 shows the derivation of equations for calculating the minimum and maximum flight speed of the solar plane. Equations 4-11 and 4-13 calculate the minimum and maximum flight velocity respectively.

Section 4-3 defines the performance parameters used to determine the performance of the solar plane during flight. These parameters can be used to determine the possibility of fight, flight time and wasted energy generation of the solar plane.

The design considerations given in 4-4 can be used to make decisions on what sort of battery should be implemented and the shape of the wings.

4-5-1 Possibilities for improvement of energy efficiency

Equation 4-25 calculates the fraction of energy that cannot be used to provide the load or charge the battery with, this value is desired to be as low as possible. In order to minimize this coefficient, this surplus energy could potentially be used to increase the flight speed or store as potential energy by increasing its flight altitude. In order for the usefulness of this functionality to be quantified the model must be expanded.

Power electronics system implementation

In this chapter the power electronics system as designed in chapter 3 will be designed and implemented on a circuit level according to specifications I1 to I3 detailed in section 2-2. This chapter will discuss the factors considered when making decisions concerning the design of the components of the power electronics subsystem. The components of which the design will be discussed in this chapter are the DC/DC converter for MPPT, the charge controller for ensuring proper power delivery to the battery and load and the voltage and current sensors.

5-1 DC/DC converter implementation for MPPT

This section will discuss the design decisions behind the DC/DC converter used for the MPPT implementation.

5-1-1 DC/DC converter implementation guidelines

In order to accommodate the varying current-voltage characteristic of the PV cell array and supply its power to the rest of the system, a DC/DC converter which can accept a varying input voltage is required. Based on initial estimates of the PV cell array layout, the output voltage of the array will be lower than that of the battery. As a result, the DC/DC converter will be a boost-converter. There are many different topologies of boost converters that can provide the desired voltage boosting functionality. The topology used for this project will be a non-synchronous switched-inductor boost converter. This design requires few components and is simple to model and should be capable of meeting the required specifications with the correct components [7]. A diagram of the circuit of a generic switched-inductor boost converter is shown in Fig. 5-1.

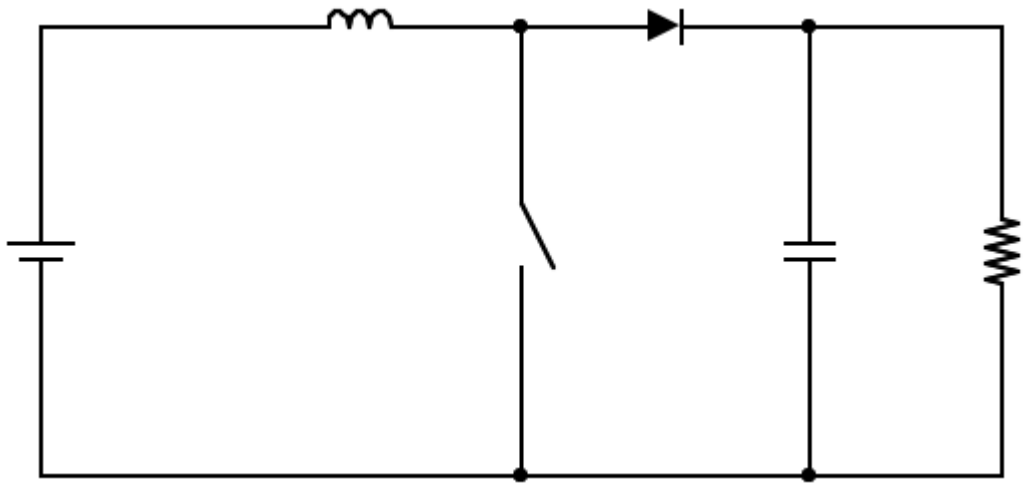

Figure 5-1: A generic switched-inductor boost converter layout

Other topologies, while more complicated, may function better at more extreme voltages, offer faster response times, improved efficiency and/or lower voltage and current ripples. However, through proper selection of components for the selected topology, the desired specifications can be met while maintaining the simplicity of the design. A simpler design also allows for the use of fewer components, which can mean a lower footprint in terms of both the weight and volume of the converter.

An important parameter of the design is the resistance of the inductor side of the converter during the 'on' period of the duty cycle. This determines how quickly the inductor current can increase as well as the maximum inductor current. A high inductor current gain is necessary in order to sustain the voltage gain at higher output currents.

A low inductor current ripple is desirable, as a change in the input current away from the desired current will cause the PV panels to operate outside of their maximum power point, meaning that incoming solar energy is being wasted. The voltage ripple on the other hand, is not of much importance. Most components connected to the system have no voltage ripple requirements and will generally remain functional as long as the supply voltage remains with the bounds of the minimum and maximum supply voltage.

The inductor current ripple is determined by the switching frequency as well as the inductance of the inductor as shown in Eq. 5-1, where D is the duty cycle, T is the period, L is the inductance and V_i is the source voltage. The output voltage ripple is determined by the switching frequency as well as the capacitance of the output capacitor, as shown in Eq. 5-2, where D is the duty cycle, T is the period, C is the capacitance, and I_o is the output current. While either ripple can be minimized by increasing the switching frequency of the converter, the switch itself may not be able to switch fast enough. A higher switching frequency can also increase the power losses in the switch, which in order to be reduced, would heavily complicate the design.

$$\Delta I = \frac{DT}{L} V_i \tag{5-1}$$

$$\Delta V = \frac{DTI_o}{C} \tag{5-2}$$

There are many different switches which can be incorporated into a boost converter. For this design an n-channel MOSFET was chosen to function as the switch due to the ability to switch on at positive voltages and the low switching times. The selection of the MOSFET itself was done by modeling and comparing the performance of various MOSFETs. The most important characteristics of the MOSFET are the conduction losses and the switching losses. The former is caused by the drain-source resistance of the MOSFET in its conducting state, while the latter is caused by the gate charge and switching times.

5-1-2 DC/DC converter design and implementation

The most important components of the switched-inductor boost converter are the inductor and the MOSFET. For the MOSFET, it is important to know how efficient the MOSFET is. If the switching times are high, the MOSFET will spend a significant amount of time in between the off and on state. Which can cause significant losses at high frequency in hard-switched converters. An illustration of this effect is shown in Fig. 5-2.

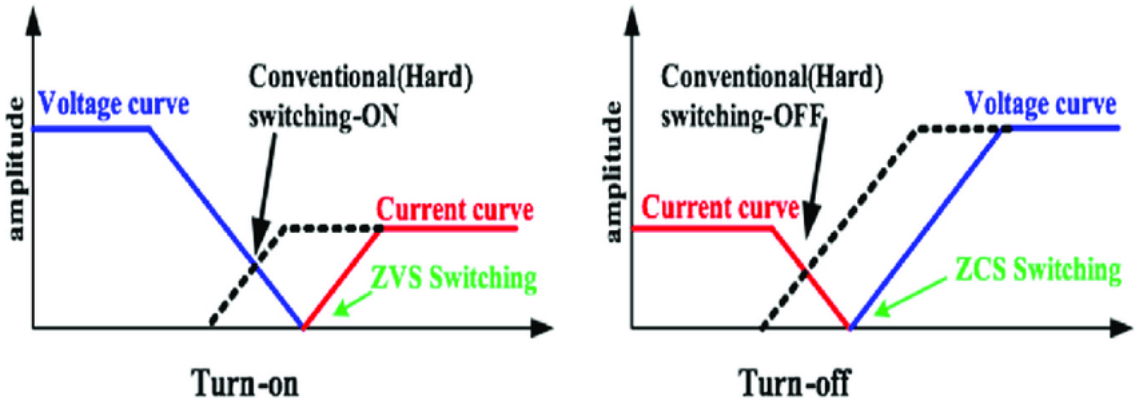

Figure 5-2: An illustration of losses caused by hard-switching compared to soft-switching. [11]

By selecting a MOSFET with low switching times (sub-50 ns) as a requirement, the time spent in this transitional state, and subsequently the losses caused by it, can be minimized for a hard-switched converter. By further calculating the conduction and switching losses at the selected operating frequency range of 100kHz - 500kHz, the optimal MOSFET for the DC/DC converter can be selected.

The conduction losses are determined by Eq. 5-3 [6]:

$$P_{CON} = R_{DS(on)} \times I^2_{SW(RMS)} \tag{5-3}$$

Where $R_{DS(on)}$ is the drain-source resistance of the MOSFET in its conducting state and $I_{SW(RMS)}$ is the RMS current going through the switch during its conducting period.

The switching losses are determined by Eq. 5-4 [6]:

$$P_{SW} = V_{DS} \times I_D \times f_{SW} \times \frac{Q_{GS} + Q_{GD}}{I_G} \tag{5-4}$$

Where the V_{DS} is the drain-source voltage, I_D is the drain current, f_{SW} is the switching frequency, Q_{GS} is the gate-source charge, Q_{GD} is the gate-drain charge, and I_G is the gate current.

With these equations, the simulated losses of various MOSFETs can be plotted as a function of the switching frequency and then compared, as shown in Fig. 5-3. The code used to calculate this data and generate these plots is included in Appendix A-3-2.

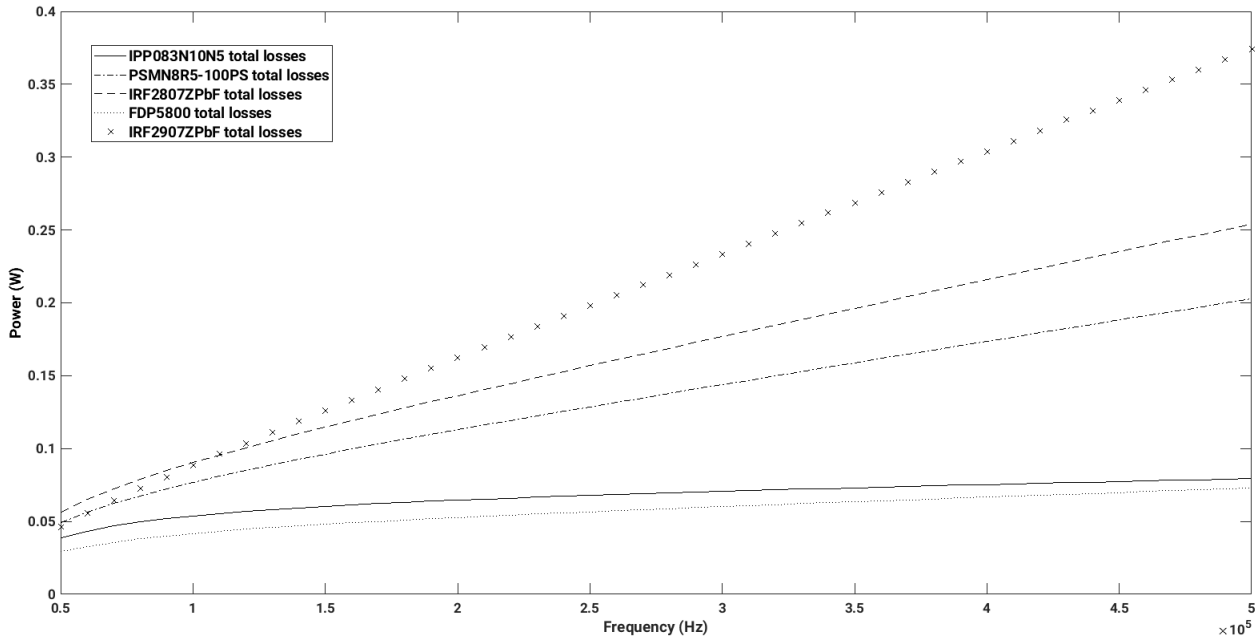

Figure 5-3: A comparison of the simulated losses in a sample of n-channel MOSFETs

Given these simulation results, the IPP083N10N5 was selected to function as the switch of the boost converter.

The important parameters of the inductor are the inductance, the DC resistance, weight and saturation current. Early estimates of the peak input current of the DC/DC converters were as high as 5A, therefore an inductor with a saturation current higher than that is required.

While there is no hard requirement for a maximum ripple current, in order to maximize the efficiency of the PV cells a maximum ripple current of 100mA was chosen. For a duty cycle of 0.5 and a switching frequency of 250kHz, a 100uH inductance gives an expected current ripple of 100mA using Eq. 5-1.

In order to ensure that the switch would be driven with sufficient gate current, the PWM signal provided by the MPPT will be amplified a gate driver which will drive the MOSFET.

The schematic of the circuit (excluding the gate driver) is given in Fig. 5-4

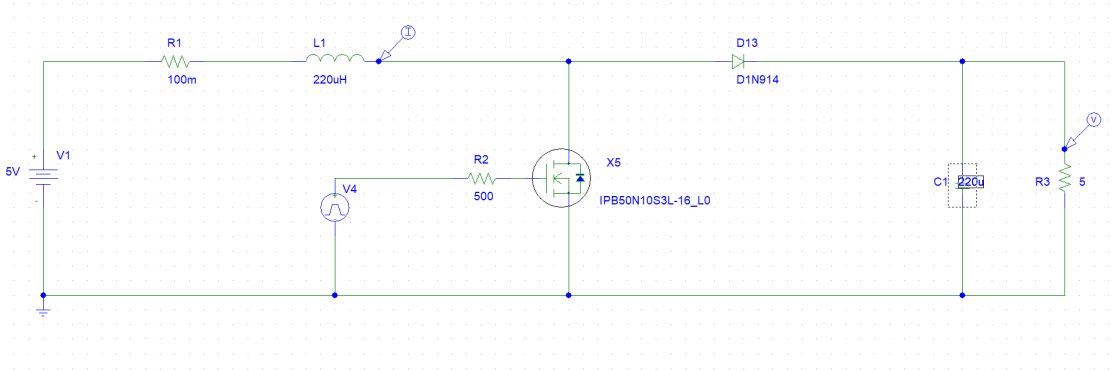

Figure 5-4: The schematic of the DC/DC converter

This design uses a higher inductance and a lower switching frequency, but the obtained SPICE simulation results (Fig. 5-5 indicate that it will be able to deliver the required while maintaining the required voltage and current ripple.

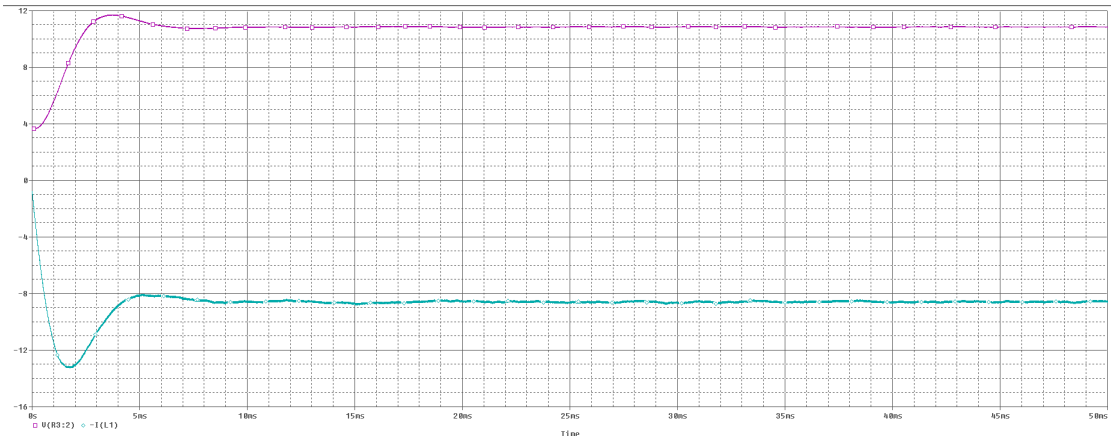

Figure 5-5: SPICE simulation results for the boost converter

5-2 Charge controller and battery implementation

This section will cover the design of the charge controller and the selection of the battery for the system.

The electrical components of the system, such as the motor and ESC have a minimum voltage requirement. This voltage is higher than the output voltage of the PV array, but the battery added to the system supplies this voltage. The voltage of this battery determines the output voltage of the DC/DC converter and as such, has been set at as low a value as possible (within the required voltage specifications of all the components of the system) as the DC/DC converter becomes less efficient as the voltage gain of the converter increases. The ESC requires a LiPo battery with a minimum of 2 cells in series giving a nominal voltage of 7.4V.

As the flight time of the plane must be extended as much as possible, the weight of the battery must be as low as possible. The battery must however, also act as an energy buffer for the

plane for when the PV array does not generate enough power. As stated in subsection 4-4-1, a battery with a high energy and power density is preferred. Figure 5-6 shows a comparison of various battery types in regards of energy and power density. The manual of the plane chassis also recommends a minimum battery capacity of 2500 mAh. However, due to the fact that the plane will be generating energy during its flight, a lower battery capacity should suffice. As a result the battery used in the design is a lithium-ion polymer battery and has a capacity of 2400 mAh.

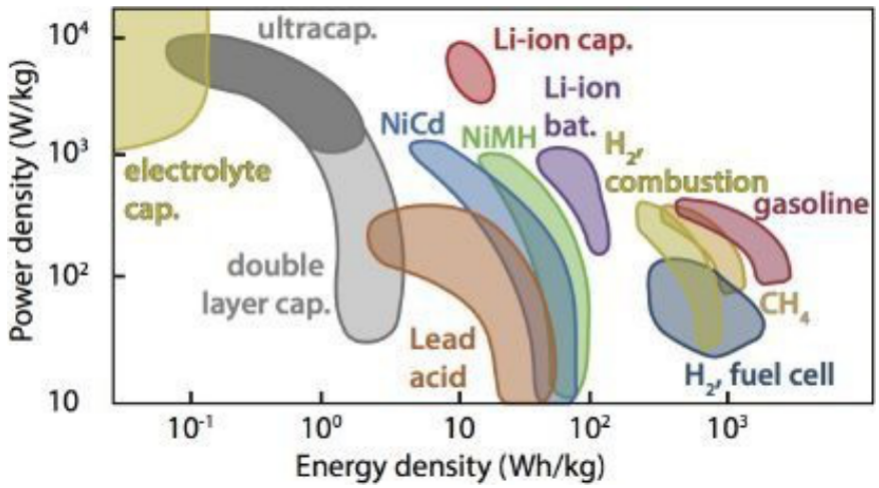

Figure 5-6: A Ragone chart of different energy storage methods. Capacitors are indicated with cap.[4]

The charge controller will consist of a load switch which is designed to disconnect the battery if the battery voltage reaches its threshold as a result of charging. It ensures that the battery will never be overcharged and that the load will always have a source of power. There is no risk of power flowing into the PV array as the DC/DC converter has a diode preventing that. The schematic of the charge controller is shown in Fig. 5-7. The voltage will be read and sent to an MCU which will also send the signal controlling the switch.

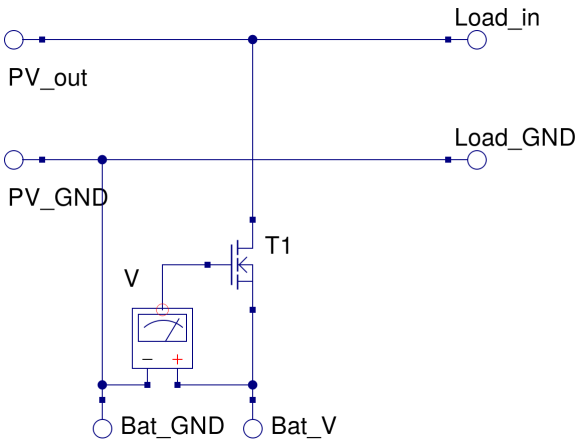

Figure 5-7: The schematic of the charge controller

5-3 Sensor implementation

For the MPPT and charge controller implementation to work as intended, the output power of the PV modules and battery must be calculated. This will be done by implementing voltage and current sensors which measurement values are read by the microcontroller MPPT and charge controller algorithms.

In this section the circuit implementations of the voltage and current sensors will be presented. The measured values of these sensors will be read by the microcontrollers and used for the MPPT and charge control algorithms.

5-3-1 Voltage sensor

In this subsection the voltage sensing circuit implementation is presented. The voltage sensor must be able to measure the voltage range given in specification I1.1 of section 2-2 and attenuate it to the voltage input range of the microcontroller $0V \leq V_{MCU} \leq V_{MCU,max}$.

Let V_{in} be the voltage measured by the voltage sensor and V_{Vsense} be the voltage read by the analog input port of the microcontroller. Figure 5-8 then presents the circuit implementation of the voltage sensor. Values for R_1 and R_2 are chosen such that equation 5-5 holds true while $R_{1,2} << R_{MCU}$.

$$0V \leq V_{Vsense} = \frac{R_2}{R_1 + R_2} V_{in} \leq V_{MCU,max} \tag{5-5}$$

5-3-2 Current sensor

In this subsection the current sensing circuit implementation is presented. The current sensor must be able to measure the current range given in specification I1.1 of section 2-2 and attenuate it to the voltage input range of the microcontroller $0V \leq V_{MCU} \leq V_{MCU,max}$.

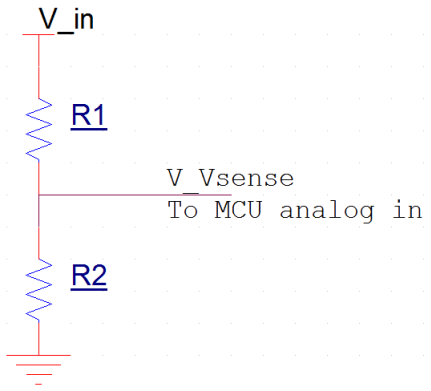

Figure 5-8: Circuit implementation of voltage sensor.

Let V_{in} be the output voltage supplied by the PV modules or battery, V_s be the voltage over R_{Isense} and V_{Isense} be the voltage read by the analog input of the microcontroller. Figure 5-9 then presents the circuit implementation of the current sensor. Values for R_1 and R_2 are chosen such that equation 5-6 holds true. Value R_{Isense} is chosen such that $R_{Isense} << R_{load}$.

$$0V \leq V_{Isense} = \frac{R_1 + R_2}{R_2} V_s \leq V_{MCU,max} \tag{5-6}$$

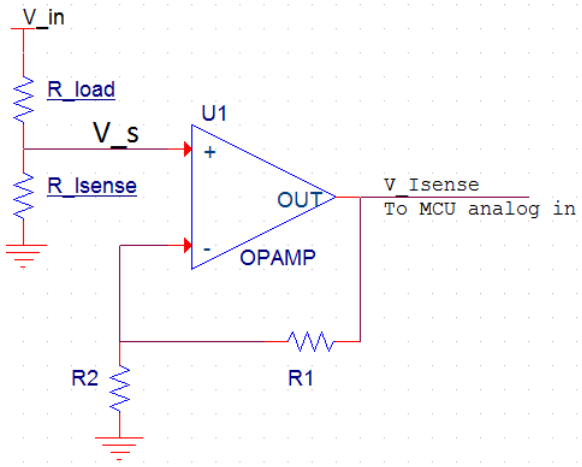

Figure 5-9: Circuit implementation of voltage sensor.

5-3-3 Sensor component selection

In this subsection the components used to realize the sensor implementations given in figures 5-8 and 5-9 will be determined.

The chosen microcontroller used for the MPPT and charge controller algorithms has an analog voltage input range of $0V \leq V_{MCU} \leq 3.3V$. Based on specification I1.1 of section 2-2 and equations 5-5 and 5-6, the component values of the sensors are given in table 5-1.

Voltage sensor	
R1	5.6 $k\Omega$
R2	2.2 $k\Omega$

Current sensor	
R1	10 $k\Omega$
R2	100 Ω
RIsense	0.1 Ω

Table 5-1: Component values for the voltage and current sensors used to measure the PV module and battery output.

5-4 Conclusion and discussion of system implementation

This chapter details the various factors taken into account when designing the various power electronics systems used in this project. The schematics for the various PE systems are also shown in this chapter.

The DC/DC converter for the MPPT will consist of a non-synchronous switched inductor boost converter capable of delivering high gain at the required output power. The charge controller will consist of a circuit connect the DC/DC converter output, battery and load, ensure that the load is always powered and that the battery is not overcharged. The design for the voltage and current sensor which will be utilized to measure the output power of the PV array and battery is also detailed.

Power electronics system modeling and testing results

In this chapter the power electronics system model of chapter 4 will be simulated and the implementation of chapter 5 will be tested in order to determine the performance of the system.

6-1 Solar plane model performance results

In this section the simulink model given in figure 4-4 will be used to evaluated the performance of the solar plane using the performance parameters defined in section 4-3 and plane component data given in table A-1. The performance parameters will be calculated for constant irradiances and simulated days starting at sunrise and high noon.

6-1-1 Determining possibility of flight

Before the plane is simulated during various irradiance profiles, the possibility of flight will be tested using performance parameter equation 4-14. The calculated minimum and maximum velocities for the solar plane with and without PV modules are given in table 6-1. Since equation 4-14 holds true for both plane configurations, the possibility of flight is determined to be plausible.

Plane without PV modules	
v_{min}	7.81 m/s
v_{max}	44.12 m/s

Plane with PV modules	
v_{min}	8.64 m/s
v_{max}	42.35 m/s

Table 6-1: Minimum and maximum flight velocities of the solar plane with and without PV modules installed

6-1-2 Performance during constant irradiance

The performance of the plane is simulated during constant irradiance I. The simulation results are given in table 6-2, the X characters imply that the plane is capable of continuous flight for the given I resulting in an theoretical infinite flight time and improvement ratio. The obtained results show that for $I \geq 200$ specification P3 is satisfied.

I	T_{flight}	$r_{T,improve}$
0	718	0.82
100	840	0.96
200	1007	1.15
300	1250	1.43
400	1638	1.87
500	2352	2.68
600	4105	4.69
700	15299	17.5
800	X	X
900	X	X
1000	X	X

Table 6-2: Flight times and improvement ratios during constant irradiance

6-1-3 Performance during simulated day irradiance profiles

The performance of the plane will be modeled during a simulated day when no shading occurs, starting in the morning and at noon. Figures A-1 and A-2 provide examples of the irradiance profiles with peak irradiance $I_{peak} = 1000$ W/m^2 starting during the morning and at noon respectively. Tables 6-3 and 6-4 yield the simulation results obtained for both time intervals. From these tables it can be concluded that specification P3 can not be satisfied when the plane is flown during the morning since $r_{T,improve} < 1$ for all irradiance profiles. If the plane is flown at noon, specification P3 is satisfied when $I_{peak} \geq 200$ W/m^2.

I_{peak}	t_{flight}	$r_{T,improve}$
0	718	0.82
100	720	0.82
200	723	0.83
300	726	0.83
400	729	0.83
500	732	0.84
600	735	0.84
700	738	0.84
800	741	0.85
900	744	0.85
1000	747	0.85

Table 6-3: Flight times and improvement ratios during simulated day starting at morning

6-2 Measuring performance of power electronics components

In this section the circuit level implementation discussed in chapter 5 will tested.

I_{peak}	t_{flight}	$r_{T,improve}$
0	718	0.82
100	839	0.96
200	1005	1.15
300	1245	1.42
400	1623	1.85
500	2297	2.62
600	3800	4.34
700	7500	8.56
800	11494	13.12
900	13386	15.28
1000	14682	16.76

Table 6-4: Flight times and improvement ratios during simulated day starting at noon

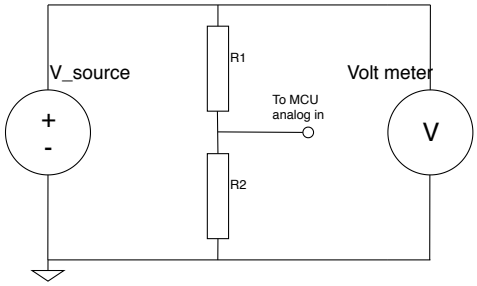

Figure 6-1: Voltage sensor test setup

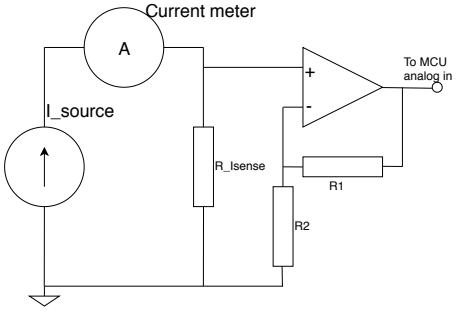

Figure 6-2: Current sensor test setup

6-2-1 Sensor testing

In this subsection the voltage and current sensors implemented in subsection 5-3 will be tested. The sensor will be considered to be working as intended if and only if the microcontroller running the MPPT and charge controller algorithms reads the correct voltage and current measured by the implementation. The sensors are required to read the measurement values within an error margin of 5% in order to be considered accurate.

Using a voltage source and current source to simulate the PV modules, the measurement setups depicted in figures 6-1 and 6-2 are used to test the voltage and current sensors respectively. The microcontroller analog input will measure the voltage V_{sensor} and current I_{sensor} values for voltage and current ranges $0V \leq V_{source} \leq 10V$ and $0A \leq I_{source} \leq 5A$, the obtained measurement values will then be compared to the measurement values of the voltage and current meters.

The percentile variance between the voltage/current meter measured values and microcontroller measured values are calculated. If all the calculated variances are lower then 5% the sensors are considered to be accurate. The obtained measurement values are given in tables 6-5 and 6-6. Since the calculated variances are all lower then 5%, the sensors are considered accurate and working as intended.

V_{source}(**V**)	0	1	2	3	4	5	6	7	8	9	10
V_{sensor}(**V**)	0.01	1.00	2.02	3.03	4.05	5.04	6.09	7.08	8.09	9.10	10.10
Variance(%)	-	0	1	1	1.25	0.8	1.5	1.14	1.13	1.11	1

Table 6-5: Measured values of voltage sensor using setup 6-1

I_{source}(**A**)	0	1	2	3	4	5
I_{sensor}(**A**)	0.02	0.98	1.98	2.99	3.98	4.98
Variance(%)	-	2	1	0.33	0.5	0.4

Table 6-6: Measured values of current sensor using setup 6-2

6-2-2 MPPT testing

The DC/DC converter was first tested with a DC power supply input with a current sensor, a 100kHz switching frequency and a 10Ω resistor load. The output voltage was measured by a multimeter. The test & measurement setup is shown in Fig. 6-3

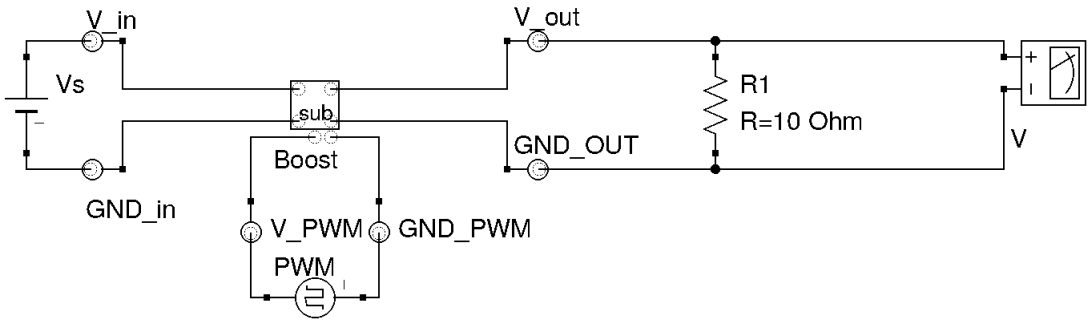

Figure 6-3: The test & measurement setup for the DC/DC converter

The converter was tested at input voltages of 5V and 6V, and a range of duty cycles from 0.2 to 0.7. The results are given in Fig. 6-4

From the results it can be seen that the converter can achieve an efficiency of up to 90% in the desired operating range. The efficiency shows a negative trend with increasing gain, so the decision to operate the system at a lower voltage will result in higher efficiency for the DC/DC converter. While the power supply used to test the system is limited to an output current of 5A, the converter was able to function properly up to at least 4.1A, which means it should be able to handle the current from the PV array.

The output voltage ripple for an input of $6V$, a duty cycle of 50% and a frequency of 100kHz was measured to be as high as $1.68V$. This causes the output voltage to shoot outside of the voltage range of the battery and electronic speed control. While there is a possibility that the output voltage does not have this ripple, as the oscilloscope used to sample this waveform showed ripple values of $300mV$ to $1.68V$, it is nonetheless, best to reduce this ripple as much as possible since outputting a voltage with a ripple this large could negatively affect the performance of the rest of the system. This could be remedied by increasing the capacitance on the output of the converter.

6-2-3 Charge controller and battery testing

The charge controller is tested by connecting the DC/DC converter to the charge controller input, and the battery and a test load to the charge controller outputs. The functionality of the charge controller can be verified if the battery voltage does not increase beyond the specified cutoff.

Unfortunately, as of the moment of writing. The charge controller components have not been delivered, and therefore the implementation of the charge controller cannot be tested.

6-3 Conclusion and discussion of obtained test results

Section 6-1 shows that during constant irradiance profile of 800 W/m^2 continuous flight can be achieved. Under simulated day irradiance profiles the flight time of the solar plane can be improved by 16.76 the planes initial flight time.

Some of the parameters used in the model are not accurately known and were therefore approximated resulting in less accurate results. Especially the drag and lift constants are of great influence on the obtained results. In order to obtain more accurate results, steps must be taken to determine the parameters more accurately.

Section 6-2 presented the acquired test results of the individual components for the implementation of the solar plane power electronics system. All tests showed the completed implementations to be working as intended, with the possible exception of the voltage ripple of the DC/DC converter.

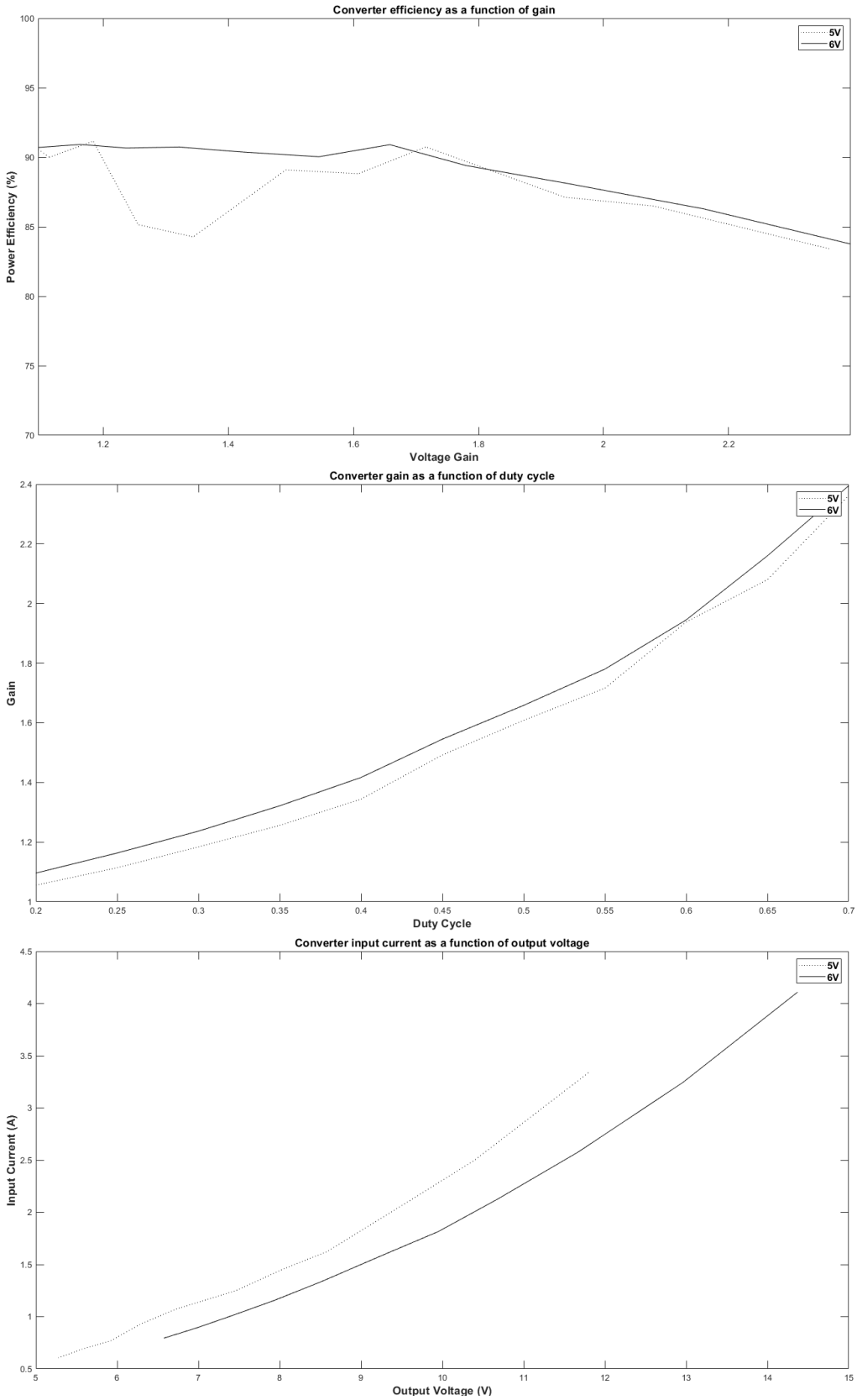

Figure 6-4: The measured values of the prototype of the DC/DC converter

Conclusion and discussion of complete system

In this thesis the power electronics system of the solar plane project was designed, modeled, implemented and tested.

Chapter 4 discussed the model, performance parameters and solar plane design considerations of the solar plane. The model was developed in order to determine the satisfaction of specifications P1 and P3 for any given solar plane configuration. The results obtained from this model and performance parameters using data of the solar plane project plane configuration are given in section 6-1.

Chapter 5 presented the implementation of the power electronics system on circuit level. This implementation was developed in accordance with specifications I1 to I3. The simulation results for the relevant components The test results of this system implementation are given in section 6-2. The results for the tested components show largely positive results, with the DC/DC converter able to deliver the necessary gain. The output voltage ripple of the DC/DC converter may possibly be outside of the required specification, and additional steps will be taken to remedy this. The charge controller was not built as of the time of writing, and therefore the functionality thereof could not be tested.

7-1 Future work

The model developed in chapter 4 only describes the plane at a constant altitude. In order to model the power usage of the plane more accurately, the model can be expanded such that it describes the take off and landing power usage of the plane as well as the power usage as varying velocities. Another addition to the model would be the method discussed in section 4-5-1.

Although design considerations for the aspect ratio of the were given in section 4-4, the project group could not use this in any meaningful way due to the inability to design their own optimal airplane wings. In order to create the most optimal solar plane, the wings must be custom made to accommodate for the most efficient PV module placement. More research should be done to determine the relation between optimal aspect ratio and PV module coverage for solar planes.

For the design of the power electronics system itself, the design of a boost converter can be improved. Currently, the standard model of the boost converter does not include the DC

resistance of the inductor and drain-source resistance of the MOSFET, although these affect the performance of the converter greatly. A model that could provide a good estimate of the performance of a boost converter as a function of a subset the various parameters of the components could make the design process of these converters much faster. A full circuit simulation that accurately simulates the MOSFETs, such as SPICE, can be impractical due to the speed of the simulation and the difference between the parameters of the MOSFET models and commercially available MOSFETs.

Bibliography

[1] A. Noth and R. Siegwart. (2006). Design of solar powered airplanes for continuous flight, [Online]. Available: https://www.ethz.ch/content/dam/ethz/special-interest/mavt/robotics-n-intelligent-systems/asl-dam/documents/projects/Design_Skysailor.pdf.

[2] T. Esram and P. L. Chapman. (2007). Comparison of photovoltaic array maximum power point tracking techniques, [Online]. Available: https://ieeexplore.ieee.org/document/4207429.

[3] B. Subudhi. (2013). A comparative study on maximum power point tracking techniques for photovoltaic power systems, [Online]. Available: https://ieeexplore.ieee.org/stamp/stamp.jsp?arnumber=6249779.

[4] O. Isabella, K. Jager, A. Smets, R. van Swaaij, and M. Zeman, *Solar Energy. The physics and engineering of photovoltaic conversion technologies and systems*. UIT Cambridge, 2015.

[5] N. Khera, N. Rana, N. S, S. K. Sahoo, B. M, S. P. Karthikeyan, and I. J. Raglend. (2015). Design of charge controller for solar pv systems, [Online]. Available: https://ieeexplore.ieee.org/document/7475266.

[6] G. Lakkas, "Mosfet power losses and how they affect power-supply efficiency", *Analog Applications Journal*, 2016.

[7] M. Forouzesh, Y. P. Siwakoti, S. A. Gorji, F. Blaabjerg, and B. Lehman, "Step-up dc-dc converters: A comprehensive review of voltage-boosting techniques, topologies, and applications", *IEEE Transactions on Power Electronics*, vol. 32, no. 12, Dec. 2017.

[8] G. Jouvet. (2017). When solar-powered drones meet arctic glaciers sun2ice, [Online]. Available: https://www.suasnews.com/2017/10/solar-powered-drones-meet-arctic-glaciers-sun2ice/.

[9] D. Karabetsky. (2017). Conceptual design of maximum power point tracking for solar rechargable airplane, [Online]. Available: https://ieeexplore.ieee.org/document/8308776.

[10] D. Karabetsky and V. Sineglazov. (2018). Analysis of solar rechargeable airplane, [Online]. Available: https://ieeexplore.ieee.org/document/8576181.

[11] M. Salem, A. Jusoh, N. R. N. Idris, H. Das, and I. Alhamrouni, "Resonant power converters with respect to passive storage (lc) elements and control techniques - an overview", *Renewable and Sustainable Energy Reviews*, vol. 91, Jun. 2018.

Appendix

A-1 Figures

A-1-1 Irradiance profiles

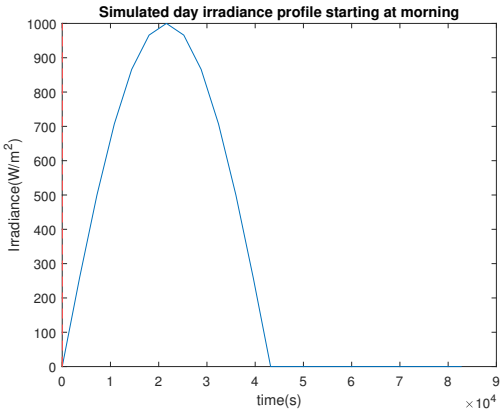

Figure A-1: Simulated irradiance profile starting in the morning and peaking at 1000 W/m^2

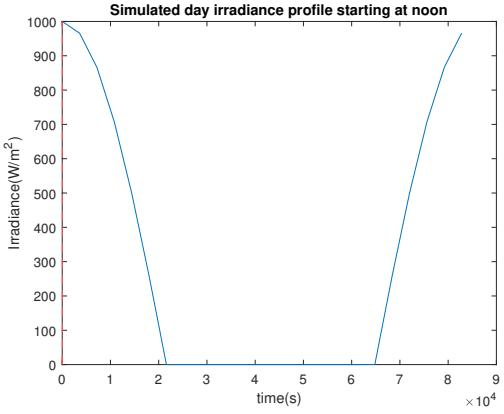

Figure A-2: Simulated irradiance profile starting in at noon and peaking at 1000 W/m^2

A-2 Tables

A-2-1 Power electronics model parameters

Plane parameters	
g	9.81 m/s^2
ρ	1.225 kg/m^3
C_L †	0.5
C_d †	0.05
A_{wings}	0.47 m^2
$k_{PVcover}$	0.9
m_{frame}	0.98 kg
m_{elec}	0.5 kg
m_{batt}	0.179 kg
ρ_{PV}	0.885 kg/m^2
n_{PV}	0.2
n_{MPPT}	0.9
$n_{Batt,charge}$ †	0.98
$n_{Batt,discharge}$ †	0.98
n_{plane} †	0.65
P_{elec}	20 W
$F_{thrust,max}$	7.848 N
C_{batt}	2400 mAh
V_{batt}	7.4 V
SOC_{max}	0.8
SOC_{min}	0.2

Table A-1: Power electronics model parameters, based on measured component values, used for simulink simulation. Parameters marked with a † symbol are approximations based on average values. The true values of these parameters are not known.

A-3 Code

A-3-1 Charge controller simulink code

```
1  %Simulink charge controller algorithm
2
3  function [P2load, P2batt] = ChargeController(P_pv, P_batt, P_load, SoC_batt)
4
5  SOC_max = 0.8;
6  SOC_min = 0.2;
7
8  if P_pv - P_load >= 0 && SoC_batt < SOC_max*100 && SoC_batt >= SOC_min*100
9      P2batt = P_pv - P_load;
10     P2load = P_load;
```

```
elseif P_pv - P_load >= 0 && SoC_batt >= SOC_max*100
    P2batt = 0;
    P2load = P_load;
elseif P_pv - P_load < 0 && SoC_batt >= SOC_min*100
    P2batt = P_pv - P_load;
    P2load = P_pv + P_batt;
else
    P2batt = 0;
    P2load = P_pv;
end
```

A-3-2 MOSFET losses simulation

```
L = 0.0001;
C = 0.0001;
R_SL = 0.1;
V_in = 5;
V_GS = [10; 10; 10; 10; 10];
I_L_av = 2;
R_load = 10;
D = 0.5;
F = 50000:10000:500000;

Transistors = ...
    ["IPP083N10N5";"PSMN8R5-100PS";"IRF2807ZPbF";"FDP5800";"IRF2907ZPbF"];
R_DS_on = [8.3; 8.5; 9.4; 6.0; 4.5] .* 10^-3;
Q_GS =[11; 24; 19; 23; 46] .* 10^-9;
Q_GD = [6.5; 33; 28; 18; 65] .* 10^-9;
Q_G = [37; 111; 110; 145; 270] .* 10^-9;
T_sw = [5; 39; 62; 14; 120] .* 10^-9;

I_ripple = D .* V_in ./(F .* L);%Ideal/Peak value
I_rms = sqrt((I_L_av - I_ripple).^2 + (I_L_av - I_ripple).^2 + ...
    (I_ripple./3).^2);
C_G = Q_G./V_GS;
DVDT_G = V_GS./T_sw;
I_G = C_G .* DVDT_G;

P_con = R_DS_on .* I_rms.^2; %Transistor resistive losses
P_sw = V_in .* I_rms .* F .* (Q_GS + Q_GD)./I_G;


Colors = ['- ';'-.';'--';': ';'x '];
for n = 1:length(Transistors)
    plot(F, P_sw(n,:) + P_con(n,:), ['k', Colors(n,:)], 'DisplayName', ...
        strcat(Transistors(n), ' total losses'));
    hold on;
end

xlabel('Frequency (Hz)');
ylabel('Power (W)');
lgd = legend;
```